A novel large-scale plasma source: two discharge modes and their correlation to the production of aqueous reactive species

2017 J. Phys. D: Appl. Phys. 50 305202

(http://iopscience.iop.org/0022-3727/50/30/305202)

IOP Publishing Journal of Physics D: Applied Physics
J. Phys. D: Appl. Phys. **50** (2017) 305202 (8pp) https://doi.org/10.1088/1361-6463/aa7a90

A novel large-scale plasma source: two discharge modes and their correlation to the production of aqueous reactive species

Bingchuan Wang[1], Dingxin Liu[1], Zhiquan Zhang[1], Qiaosong Li[1], Zhijie Liu[1], Li Guo[1], Xiaohua Wang[1] and Michael G Kong[1,2,3]

[1] State Key Laboratory of Electrical Insulation and Power Equipment, Centre for Plasma Biomedicine, Xi'an Jiaotong University, Xi'an City 710049, People's Republic of China
[2] Frank Reidy Center for Bioelectrics, Old Dominion University, VA 23508, United States of Ameria
[3] Department of Electrical and Computer Engineering, Old Dominion University, Norfolk, VA 23529, United States of Ameria

E-mail: liudingxin@mail.xjtu.edu.cn and mglin5g@gmail.com

Received 17 December 2016, revised 11 June 2017
Accepted for publication 20 June 2017
Published 11 July 2017

Abstract

In this paper, a novel large-scale plasma source is put forward, which can generate two modes of discharge, i.e. the surface dielectric barrier discharge and the plasma jet array, by just varying the helium gas flow rate. It is found that the discharge power changes a little with the increasing gas flow rate, but the densities of reactive species in the gas phase and in the treated water change a lot. In particular, the gaseous O_3 has its density decreasing while the aqueous O_3 has its concentration increasing with the increasing gas flow rate. In the plasma-treated water, the reactive nitrogen species such as nitrite and nitrate have their concentrations first increasing and then decreasing, while the reactive oxygen species such as H_2O_2, O_3 and OH have their concentrations increasing monotonically, implying that the plasma source is well-adaptive for different application requirements.

Keywords: surface dielectric barrier discharge, jet array, reactive species, plasma–liquid interaction

(Some figures may appear in colour only in the online journal)

1. Introduction

Cold atmospheric-pressure plasmas (CAPs) are suitable for the treatment of heat-sensitive and/or vulnerable objects that cannot withstand high temperature or low pressure, such as liquids and living tissues [1]. Thus, they have shown great prospects in diverse application fields including biomedicine [2–5], water purification [6] and nanotechnology [7]. For many of these applications, CAPs are preferable to have a large area of at least several square centimeters, because in that case some objects such as a bleeding wound can be treated wholly and in time. However, CAPs such as a plasma jet typically have a cross-section of less than one square centimeters [8], and hence they need to be scaled up to meet the application requirements. Furthermore, CAPs are preferable to produce reactive species efficiently, since some of them such as OH, H_2O_2 and O_3 are widely thought to play a dominant role in applications [3]. In particular, for the liquids and living tissues that to be treated, the production efficiency of aqueous reactive species, instead of that of gaseous ones, is significant, because it is mainly the aqueous species that acting on the targets in moisture circumstance [2, 5]. So far, there are many reports aimed at the measurement and/or the enhancement of the production efficiency of gaseous reactive species [9–12], but little is for the aqueous reactive species due to the big knowledge gap in plasma–liquid interaction [13].

Several kinds of large-scale CAP sources have been developed in the last decade, among which the surface dielectric barrier discharge [14–17] and the plasma jet array [18, 19] are very popular. The former is easy to generate very thin plasma

(thickness <1 mm [20]) over an area of hundreds square centimeters, and open air can be used as the working gas which is chemically active and no-cost [21, 22]. Various kinds of reactive species can be generated, but some of them have low possible to act on the treated object because their lifetimes are very short but the object is normally several millimeters away from the surface plasma. For example, it is predicted that the diffusion distance of atomic oxygen during its lifetime is less than 1 mm [23]. Different to the surface dielectric barrier discharge, the plasma jet array normally has plasma plumes of several centimeters long and hence could be in contact with the treated objects [24]. In that case, more short-lived reactive species including electrons and ions can act on the targets, implying that the plasma jet array is more suitable for some applications where the short-lived species are important. However, noble gas flow is normally needed for the generation of plasma jet array, which is expensive, and it is not easy to keep homogeneity among the plasma plumes [25]. The two kinds of large-scale plasmas each have advantages and disadvantages, and hence a CAP source which can generate both kinds of plasmas would be more adaptive for different applications.

In this paper, we report a novel large-scale plasma source, which can be operated in two discharge modes, namely the surface dielectric barrier discharge and the plasma jet array, by simply varying the flow rate of helium gas. A petri dish of deionized water is put underneath the plasma source for studying the plasma–liquid interaction, especially the production of aqueous reactive species including OH, H_2O_2, O_3, nitrite (HNO_2/NO_2^-) and nitrate (HNO_3/NO_3^-). These aqueous species are commonly reported to be generated by CAPs, and they are widely thought to have strong biological effects [2]. However, so far the correlation between the production efficiency of aqueous species and the characteristics of gas plasmas is unclear, which hinders the tailoring and improvement of the CAP sources for the treatment of water-containing objects [26]. In this paper, the discharge mode transition with the increasing gas flow rate, and the relevant changes in the plasma characteristics, such as the discharged image, the emission spectrum as well as the density of gaseous ozone will be presented, and the underlying mechanism will be discussed. Moreover, emphasis will be made on the correlation between the gas plasma modes and the production efficiencies of aqueous reactive species, with the purpose of deepening the understanding of plasma–liquid interaction.

2. Experimental setup

The schematic diagram of the experimental setup used in this study is illustrated in figure 1. The large-scale plasma source consists of a high-voltage (HV) mesh electrode sealed by silicone rubber, a grounded mesh electrode, a slice of ceramic plate (1 mm thickness) sandwiched between the two electrodes, and a gas chamber with a flow equalization board therein. Both the silicone rubber and ceramic plates have several arrays of small holes (a total of 33 holes), and each of them has a diameter of 0.8 mm. This allows gas flowing from the gas chamber to the open air, and the flow equalization board is used to keep the hole-to-hole homogeneity of the gas flow. Correspondingly, the HV electrode has 33 larger holes with a constant diameter of 4 mm, and it is well sealed by silicone rubber to avoid the possible flashover to the ground electrode. The ground electrode has 33 hexagon mesh elements, and each side of an element has 4 mm in length, 0.76 mm in width, and 0.5 mm in thickness. Each small hole of the ceramic plate is located in the center of a larger hole of the HV electrode and an element of the ground electrode. The HV electrode was connected to a sinusoidal power source with a constant frequency of 20 kHz, and the applied voltage was held at a peak-to-peak value of 5 kV. Helium with high purity (5 N) was controlled by a mass flow controller to flow through the holes with a total gas flow rate of 0 (helium is not used), 2, 4 and 8 SLM (standard liters per minute), respectively.

The discharge voltage was measured by a high voltage probe (Tektronix, P6015A), and the discharge current was measured by a current probe (Tektronix, P6021). The discharge current contains the displacement and conduction components. Their waveforms were recorded by an oscilloscope (Tektronix, MDO3054), and the discharge powers were obtained by integrating the product of voltage and current. The plasma images were taken by a digital camera (Nikon, D7000) with an exposure time of 0.8 s, while the time-resolved plasma images were taken by an intensified CCD camera (Andor, iStar DH334) with an exposure time of 100 ns. The emission spectra of the plasmas were detected by a spectrometer (Andor, Shamrock 750i). Besides, an ultraviolet (UV) power probe, connected to an ultraviolet power photometer (International Light Technology, model IL1400A), was put 20 mm away from the ground electrode to measure the UV power of the plasma.

A petri dish of deionized water (8 ml) was put 5 mm underneath the plasma source (not shown in figure 1) to study the plasma–liquid interaction. The densities of reactive species were measured both in the gas phase and the liquid phase. In the gas phase, the ozone density was measured by means of UV absorption spectroscopy as widely used in the literature [27]. A deuterium lamp (Ocean Optics, DH2000) was used to produce a line light across the downstream area of the plasma, parallel to and at 5 mm below the mesh electrode. The spectral line of $\lambda = 253.75$ nm was recorded by the spectrometer. In the liquid phase, the density of ozone was measured by a spectrophotometer (Hach, DR3900), for which an indigo reagent (AccuVac@ Ozone Reagent, Low Range 0–0.75 mg l^{-1}) was utilized and the absorption spectral at $\lambda = 600$ nm was detected. It should be noted that the liquid volume was changed to be 1 ml for the measurement of aqueous ozone because its concentration is lower than the detection limit when the volume is 8 ml.

The pH value was measured by a pH probe (Sartorius, PB-10), and it would reflect the density of H^+. The concentrations of H_2O_2, nitrate, and nitrite were detected by using a microplate reader (Thermo Scientific Varioskan® Flash Reader). The Amplex® Red reagent was added into the deionized water after the plasma treatment, and it reacted with H_2O_2 in a 1:1 stoichiometry to produce the red-fluorescent oxidation

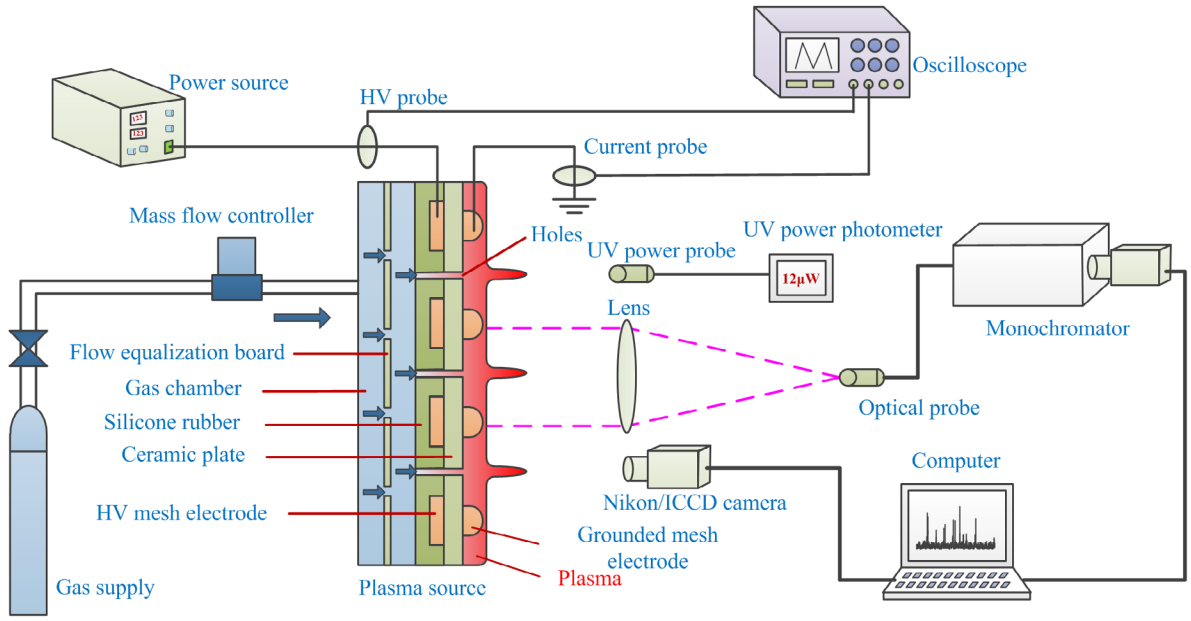

Figure 1. Schematic diagram of the experimental setup.

product, which was excited at $\lambda = 550$ nm and emitted at $\lambda = 595$ nm. For the detection of nitrite, the Griess reagent was added into the water, and the absorbance was measured at $\lambda = 540$ nm. After that, a nitrate reductase enzyme and Griess reagent were added into the water to measure the total concentrations of nitrate and nitrite at the same spectral wavelength. Finally, the nitrate concentration was obtained by subtracting the nitrite concentration from the total concentration of nitrate and nitrite, similar to those reported in the literature [23, 28, 29]. The O_2^- and OH radicals were measured by using an X-band electron spin spectrometer (BrukerBioSpin GmbH, EMX), for which the 5, 5-dimethyl1-py-rrolineN-oxide (DMPO) of 200 mM was added to the deionized water prior to plasma treatment. The spin adduct of DMPO-OOH was generated by the reaction between DMPO and O_2^-, while the spin adduct of DMPO-OH was generated by the reaction between DMPO and OH. It is noted that DMPO-OOH immediately decays to DMPO-OH, which has a special feature with a peak intensity ratio of 1:2:2:1. Hence, the signal of DMPO-OH represents the total concentrations of O_2^- and OH. More details about the techniques and the experimental procedures were reported previously [30].

The experiments for plasma treatment were carried out in an open environment with a relative humidity of 68%. The reactive species were measured right after the plasma treatment of 3 min. All measurements were repeated three times to obtain an error bar in favor of the statistical analysis. The height of each error bar represents the average measured concentration with the standard derivation.

3. Results and discussion

Plasmas are generated in each mesh element of the ground electrode when the high voltage is applied, which totally cover a large area of ~17.5 square centimeters. The plasma images in local areas of the ground electrode are shown in figure 2 for the helium flow rates of 0, 2, 4 and 8 SLM, respectively. Although the applied voltage is held at a peak-to-peak value of 5 kV for all cases, the plasma images change significantly with the variation of helium gas flow. When the gas flow rate is no more than 2 SLM, the discharge is obviously in the mode of surface dielectric barrier discharge. Filamentous plasmas are generated along the sides of each hexagon elements, and their emission intensity increases with the gas flow rate. This might be attributed to the fact that the electrical breakdown voltage of helium is lower than that of air [31], and hence the discharge intensity increases with the additive helium in the air. More details about the similar surface discharges in helium and/or air, please refer to our previous reports [29, 32]. When the gas flow rate is increased to at least 4 SLM, plasmas are generated in the small holes as shown in figures 2(c1) and (d1). Such plasmas are in the mode of plasma jet array, as shown clearly in figures 2(c2) and (d2). The plasma jets have a very good jet-to-jet homogeneity, and their lengths increase with the gas flow rate. As shown in figure 2(d3), the length of a plasma plume is ~6 mm for the gas flow rate of 8 SLM, corresponding to only ~0.26 SLM per each hole. In such cases, the surface discharge along the sides of each hexagon elements is inhibited, since the emission intensity decreases with the increasing helium gas flow rate. Therefore, it could be concluded that the discharge mode changes from a typical surface dielectric barrier discharge to a jet array-dominant discharge with the increasing helium gas flow.

In order to understand the spatiotemporal evolutions of the plasmas, the luminous patterns in a single mesh element under the helium flow rate of 8 SLM taken by the ICCD camera with an exposure time of 100 ns are shown in figure 3. The waveforms of discharge voltage and current during one cycle are also shown in figure 3, of which the time is corresponding to the captured moment of each luminous pattern as presented there. In the positive half cycle of the applied voltage, the first

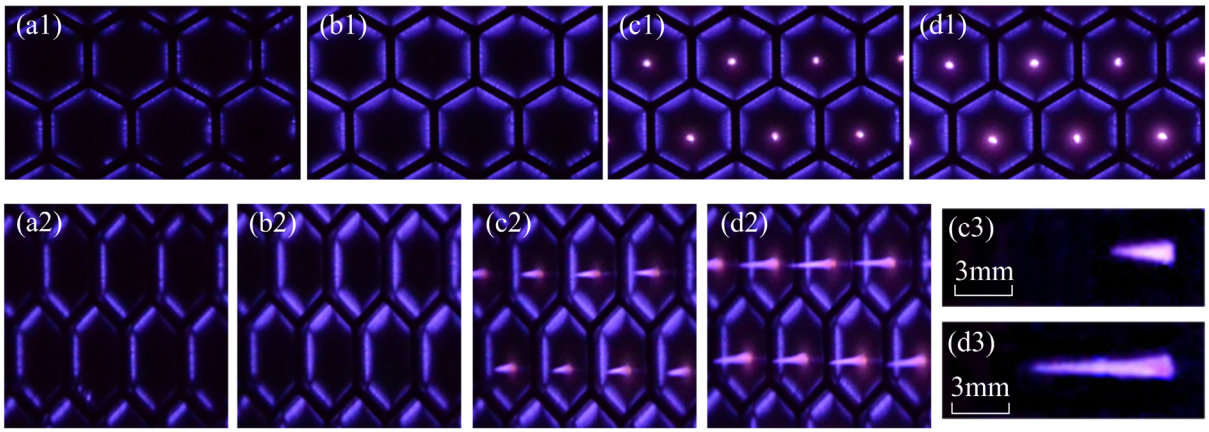

Figure 2. The plasma images were taken by a digital camera for the helium flow rates of 0 SLM (a1) and (a2), 2 SLM (b1) and (b2), 4 SLM (c1)–(c3) and 8 SLM (d1)–(d3). (a1)–(d1) are the front views of the plasmas in local area, (a2)–(d2) are taken by the camera at 30° angles to the electrode surface, and (c3) and (d3) are the side views of the plasmas in one mesh element.

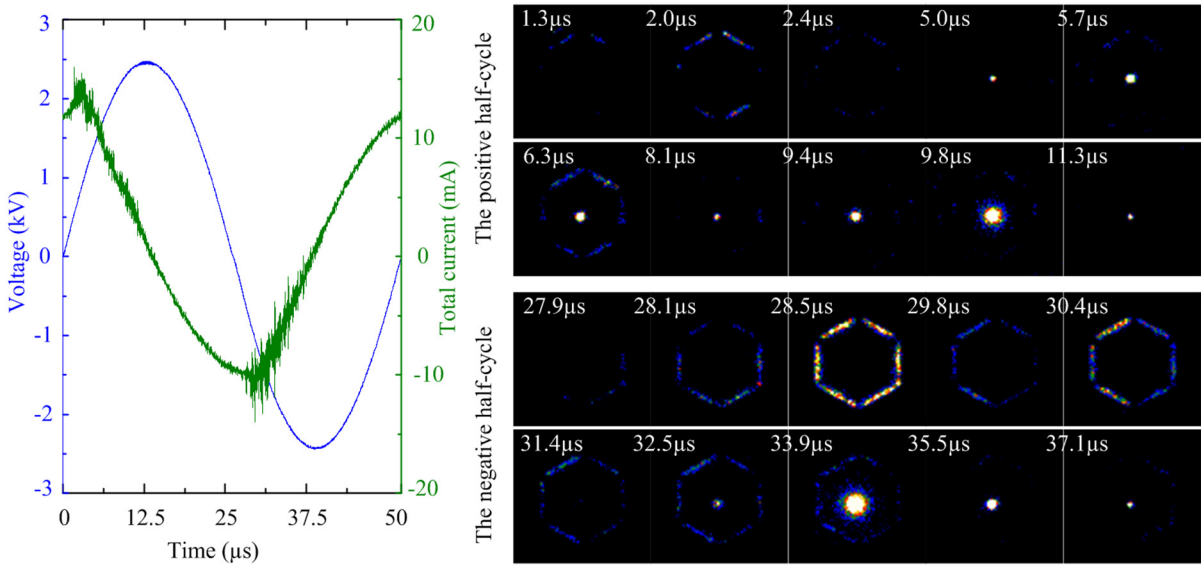

Figure 3. Waveforms of the discharge voltage and current, as well as the time-evolution of the discharge pattern in a mesh element. The helium flow rate is 8 SLM, and the exposure time for the images is 100 ns.

discharge occurs in the edge region of the mesh element at the instant of ~1.3 μs, and it lasts for only 1.1 μs before its disappearance. About 2.6 μs afterward (at the instant of ~5.0 μs), a second discharge occurs in the center part of the mesh element, i.e. in the small hole where helium flows through. The intensity of the discharge first increases and then decreases from ~5.0 μs to ~8.1 μs, and during this period the discharge is also ignited in the edge region of the mesh element. Afterward, the discharge in the center part of the mesh element has its intensity increasing again, and the luminous pattern becomes largest at the instant of ~9.8 μs. The discharge decreases then and disappears at the instant of ~11.3 μs.

In comparison, the time evolution of the luminous patterns in the negative half cycle of the applied voltage is much different. The discharge in the edge region of the mesh element occurs at the instant of ~27.9 μs, and it lasts for ~3.5 μs before the discharge in the center part occurs. Afterward, the discharge in the edge region has its intensity decreasing, while the discharge in the center part has its intensity increasing first to the instant of ~33.9 μs and then decreasing. The discharges in both the edge region and the center part disappear at the instant of ~37.1 μs.

Interestingly, the discharges in the center part of the mesh element lag behind that in the edge region by ~3.6 μs in both positive and negative half cycles. Considering that the breakdown voltage in helium is much lower than that in the air, this indicates that the local electric field in the edge region is much higher than that in the center part. However, the discharge in the edge region disappears earlier, which may because the air is electronegative and hence the electrons disappear more quickly.

The emission spectra of the plasmas are shown in figures 4(a) and (b) for the gas flow rate of 0 SLM and 8 SLM, respectively. The main spectra lines are marked with the corresponding species in the figure according to the literature [33–35]. It can be seen that the main radiative species are OH(A), N_2(C), N_2^+ (B), N_2(B), He(3^1P), He(3^3D), He(3^1D), He(3^3S) and O(^{3}P) for the helium gas flow of 8 SLM, while

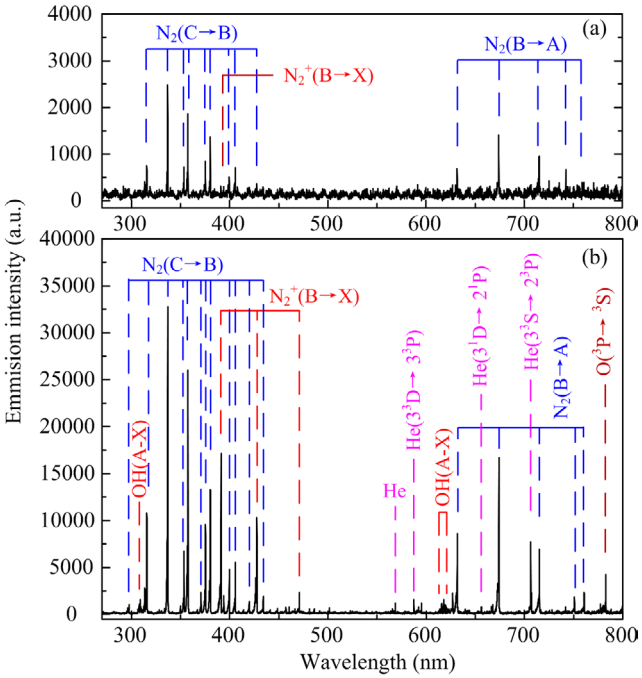

Figure 4. Emission spectra of the plasmas under the helium flow rates of (a) 0 SLM and (b) 8SLM.

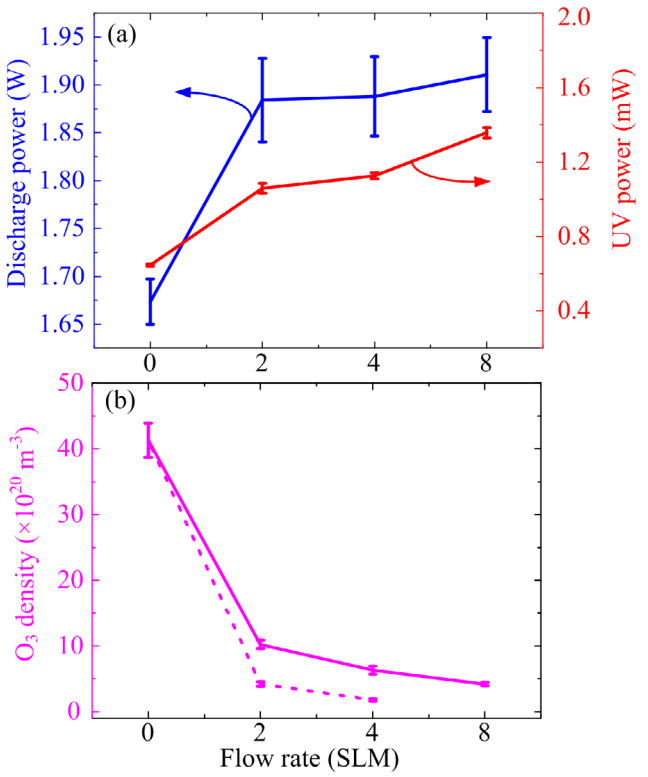

Figure 5. Dependence of the discharge power and the UV power of the plasma (a), as well as the O_3 density in the gas gap (b) on the gas flow rate. The measurements are carried out at the plasma on time of 3 min. The dashed curve in (b) represents the O_3 density as a function of air flow, instead of helium flow for comparison.

for air (gas flow = 0 SLM) only the emission spectrum of $N_2(C)$ and $N_2^+(B)$ is detected. The emission intensity of a spectral line could reflect the density of a radiative species, and it should be noted that for the measurements all the experimental conditions were kept the same except for the gas flow rate. As shown in figures 4(a) and (b), the spectral intensity of $N_2(C)$ increases by ~13.2 fold as a result of the helium gas flow of 8 SLM. This implies that a larger amount of reactive species is produced when the air is mixed with helium.

For atmospheric plasma, the gas temperature is close to rotational temperature [36]. Based on the emission spectrum, the rotational temperature of the plasma was obtained by fitting the measured and simulated spectra of the N_2 first negative system from 386 to 392 nm. The rotational temperature of the plasma is ~330 K for all the gas flow rates.

The air mixed with helium also leads to increases in discharge power and UV power, as shown in figure 5(a). The discharge power increases by ~1.1 fold with the gas flow rate from 0 to 2 SLM, and then it basically keeps constant of ~1.9 W. In comparison, the UV power keeps increasing by almost ~2.1 fold with the gas flow rate from 0 to 8SLM. Different to the discharge power, the density of O_3 in the downstream region decreases monotonically with the increasing helium gas flow rate. As illustrated by the solid curve in figure 5(b), ozone has a large density of ~4.2×10^{21} m^{-3} without the mixture of helium, but it decreases by approximately one order of magnitude with the helium gas flow rate of 8 SLM. Several reasons would be responsible for such a trend, but the main one should be that more O_3 molecules are blown away to the surrounding space with the increasing gas flow rate. In order to evaluate the influence of this reason, a comparative experiment was carried out in which the air flow was used instead of the helium gas flow. The results are illustrated by the dashed curve as shown in figure 5(b). It should be noted that the discharge power and the emission spectrum are nearly invariable with the air flow when it is not strong as reported previously [29], indicating that the yield of reactive species including O_3 does not change much. However, when the gas flow rate is as large as 8 SLM the homogeneity of plasma will be destroyed, and hence the corresponding O_3 density is not shown here. According to the dashed curve in figure 5(b), the density of O_3 decreases by nearly one order of magnitude with the increasing air flow from 0 to 4 SLM, more pronounced than that for the helium gas flow (the solid curve). This indicates that the gas blow is the main reason for the decline of O_3 density in the gas region underneath the plasma source. Other reasons such as the increase of UV power (UV photon is capable of dissociating O_3) must have little influence since the UV power is low.

The plasma-generated gaseous species will dissolve into the deionized water and then react with the water molecules to generate various aqueous reactive species [38]. The plasma-induced aqueous reactive species include the long-lived species such as nitrate, nitrite, H_2O_2, O_3 and H^+, and the short-lived species such as OH, as widely reported in the literature [4, 37]. Here, the concentrations of nitrate, nitrite, H_2O_2 and O_3 in the plasma-treated deionized water are shown in figure 6, as a function of the helium gas flow rate. Besides, the density of DMPO-OH and the pH value are also shown in figure 6, which can reflect the relative density of the aqueous

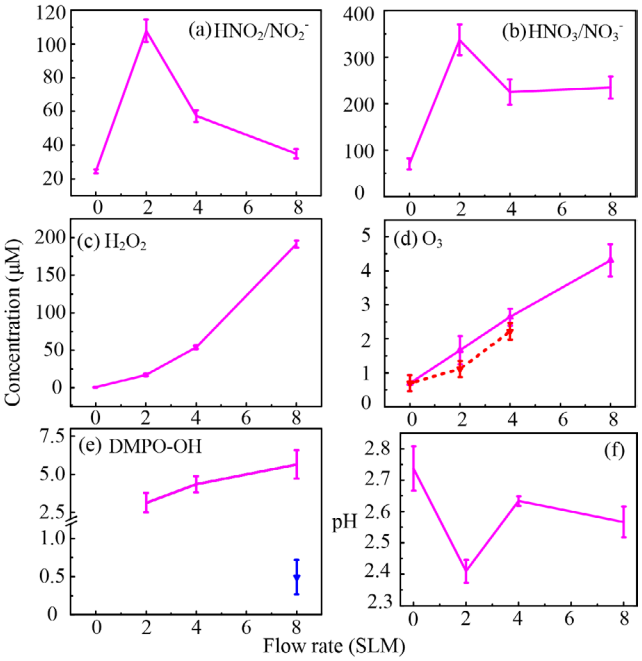

Figure 6. Concentrations of nitrate, nitrite, H_2O_2, DMPO-OH, and O_3 in the deionized water, as well as the pH value of the water as a function of the helium flow rate. The plasma treatment time is 3 min. The pink curve in (a)–(f) represents the concentrations and the pH value as a function of helium flow rate. The dashed curve in (d) represents O_3 concentrations as a function of air flow, instead of helium flow for comparison. The blue point in (e) represents the measured DMPO-OH concentration when DMPO was added into the water right after plasma treatment. The pH value of the untreated solution is about 7.2 in (f).

OH and the absolute density of H^+ ($pH = -\lg([H^+])$), respectively. It should be noted that the typical electron spin resonance spectrum of DMPO-OH was not detected in the case of no gas flow, which might be ascribed to the disturbance of other reactive species such as O_3^- [38].

As shown in figures 6(a) and (b), the concentrations of nitrite and nitrate first increase and then decrease with the increasing helium gas flow rate. Both of the concentrations peak at the gas flow rate of 2 SLM. On contrast, the concentration of aqueous H_2O_2 increases monotonically by ~237 fold with the helium gas flow rate from 0 to 8 SLM (figure 6(c)). Because these three species have high solubility (Henry's coefficients are larger than 1000 [23]), their densities should have similar trends in the gas and liquid phases. Therefore, it could be deduced that the densities of gaseous HNO_2 and HNO_3 first increases and then decreases with the helium gas flow rate. Similar to H_2O_2, the concentrations of OH and O_3 also increases monotonically with the helium gas flow rate (see figures 6(d) and (e)). So, it can be concluded that the reactive nitrogen species (mainly nitrite and nitrate) and reactive oxygen species (including H_2O_2, OH) have different trends to the gas flow rate. This implies that the biological effect of the discharge source could be regulated to a large extent by just varying the gas flow rate because these two types of reactive species have different biological functions [3]. The increase of gas flow rate from 2 SLM to 8 SLM did not lead to sharp decrease of the density of reactive nitrogen species in our experimental conditions (figures 6(a) and (b)), but for some applications where reactive nitrogen species are not preferrable, one could additionally use shielding gas such as O_2 around the discharge source to avoid the participation of N_2 in the working gas, and consequently decrease the production of reactive nitrogen species sharply [39].

Interestingly, the density trend of aqueous O_3 is opposite to that of the gaseous one as shown in figure 5(b). We hypothesize that this is because Henry's coefficient of ozone is just 0.2298 which strongly inhibits the dissolution [40], and hence the renewal of the water surface by the gas blow can greatly accelerate its dissolution process. The renewal of water surface under a plasma jet has been reported in the literature [41, 42]. In order to validate the hypothesis, the aqueous O_3 concentrations were also measured for the air flow rates of 0, 2 and 4 SLM, as illustrated by the dashed curve in figure 6(d). It can be seen that the concentration of aqueous O_3 increases with the air flow rate, opposite to the density of gaseous O_3 as illustrated in figure 5(b). So, the reverse trend between the densities of gaseous and aqueous O_3 is mainly attributed to the gas blow, not the additive of helium in the air and the corresponding change in heterogeneous chemistry. It should be noted that the indigo assay could react with other reactive oxygen species such as H2O2 and OH. But O3 reacts extremely rapidly with indigo under acidic conditions, and the interference from other reactive oxygen species can be masked for short lifetimes or are negligible because of slow rates of reactions [43]. For example, we tried to use a water solution with hydrogen peroxide concentration of 1 mM to test its influence on the indigo assay, and no fluorescence signal was detected. The concentration is much larger than that in the plasma-activated water (see figure 6(c)), indicating that the influence of hydrogen peroxide on the indigo assay could be neglected. We also tested the interference of OH on the indigo assay by preparing a solution with 200 μM $FeSO_4$ and H_2O_2, and then putting indigo blue reagent into the solution after 5 min. A large amount of OH (~200 μM) would be generated in the solution by Fenton reaction [44], but no fluorescence signal was detected. Moreover, OH radical has a short lifetime, so after plasma treatment, the concentration of OH would decrease sharply. This is verified by the DMPO-OH concentrations for the gas flow rate of 8 SLM as shown in figure 6(e). The measured DMPO-OH concentration is more than 5 μM when the reagent (DMPO) is added into the water before plasma treatment, but it is lowered by one order of magnitude when DMPO is added into the water right after plasma treatment. Since the indigo reagent is added into the water after the plasma treatment, the influence of OH radical on the indigo assay would also be negligible. So, the indigo assay results largely reflected the concentration of aqueous O_3 although it is interfered by some other species. O_3 has been predicted to play a dominant role for sterilization, and our findings may explain why the antibacterial effect of a surface discharge is significantly enhanced by vortexing the bacterial suspension [4].

The concentration trend of DMPO-OH is shown in figure 6(e), which reflects the relative concentration of aqueous OH and O_2^- as discussed in the literature [45]. There might be three pathways for the production of aqueous OH:

The first is the dissolution of gaseous OH which might be important only when the plasma is very close and/or in contact with the water surface. According to [46], the dissolved OH radical would strongly react with water molecules through hydrogen-abstraction reaction:

$$OH + H_2O \overset{aq}{\leftrightarrow} [HO - H - OH] \overset{aq}{\leftrightarrow} H_2O + OH. \quad (R1)$$

This reaction does not consume the OH radical because the product is also OH, so it may penetrate into the water to a certain depth. The gaseous OH can be generated by dissociation of water vapor in the plasma, and the water vapor could be supplied by the open air and the evaporation of the water. Because the lifetime of gaseous OH is a few milliseconds at atmospheric pressure conditions [48], the produced OH radicals are immediately decreased by reacting with other gaseous species, and hence the dissolution could be enhanced when the plasma is more close to the water. In addition, the evaporation of the water would increase with the helium gas flow rate, which is preferable for OH production because the working gas is more humid above the liquid surface. Therefore, more gaseous OH can dissolve into the water due to the extension of the plasma plume.

The second is the dissociation of liquid water molecules via energetic particles generated by the plasmas, as follows [47–51].

$$H_2O + P \rightarrow OH + H + P \quad (R2)$$

where P represents an energetic particle such as an electron, a VUV photon or an excited helium atom. For example, the bond energy of HO–H is 498.7 kJ mol^{-1} (5.17 eV) [52], and the plasma-generated VUV photon could have an energy of 9.84 eV, so it is capable of decomposing H_2O to form OH radical [49]. According to figures 2(c3) and (d3), the length of the plasma plume increases with the helium gas flow rate. Especially in the case of 8 SLM, the plasma plume is contacted with the liquid surface. In that case, more hydroxyl radicals can be produced by the energetic particles since their lifetimes are very short.

The third is the liquid chemistry with the reactants of HO_3, H^+, O_3^-, etc. These reactants are generated in the water but fundamentally they are induced by the plasmas, so the liquid chemistry mainly happens in the interfacial layer of the water [38]. The main liquid reactions are as follows:

$$HO_3 \rightarrow OH + O_2 \quad (R3)$$

$$H^+ + O_3^- \rightarrow OH + O_2. \quad (R4)$$

These liquid reactions would extend the existence time of OH radical in the water, as can be verified by the detectable DMPO-OH concentration of ~0.5 μM when DMPO is added after the plasma treatment.

4. Conclusions

In this paper, a novel large-scale plasma source is put forward, which can generate two modes of discharge, i.e. the surface dielectric barrier discharge and the plasma jet array, over an area of ~17.5 square centimeters. The switch between the two discharge modes can be easily realized by varying the helium gas flow rate. It is found that the density of some radiative species such as OH(A) increase with the increasing helium gas flow rate, but other kinds of reactive species such as O_3 has its density decreasing due to the gas blow. On contrast, the aqueous O_3 has an opposite density trend to its gaseous counterparts, which is because the solubility of O_3 is very small and hence the renewal of water surface by gas blow greatly enhances its dissolution. The discharge power is found to change a little with the increasing helium gas flow, but the plasma-induced aqueous reactive species have their concentrations change a lot. In particular, the reactive nitrogen species such as nitrite and nitrate have their concentrations first increasing and then decreasing, while the reactive oxygen species such as H_2O_2, O_3, and OH have their concentrations increasing monotonically. Since the reactive oxygen species and reactive nitrogen species have different biological effects, this implies that the plasma source has a good adaptive capacity for different application requirements.

Acknowledgment

This work was supported by the National Science Foundation of China (Grant No. 51677147 and 51561065), the Fundamental Research Funds for the Central Universities and the State Key Laboratory of Electrical Insulation and Power Equipment (Grant No.EIPE14129).

ORCID

Dingxin Liu https://orcid.org/0000-0002-3503-9883

References

[1] Stoffels E, Sakiyama Y and Graves D B 2008 *IEEE Trans. Plasma Sci.* **36** 1441–57
[2] Xu D, Liu D, Wang B, Chen C, Chen Z, Li D, Yang Y, Chen H and Kong M G 2015 *PLoS One* **10** e0128205
[3] Kong M G, Kroesen G, Morfill G, Nosenko T, Shimizu T, van Dijk J and Zimmermann J L 2009 *New J. Phys.* **11** 115012
[4] Pavlovich M J, Chang H W, Sakiyama Y, Clark D S and Graves D B 2013 *J. Phys. D: Appl. Phys.* **46** 145202
[5] Zhong S Y, Dong Y Y, Liu D X, Xu D H, Xiao S X, Chen H L and Kong M G 2015 *Br. J. Dermatol.* **10** 14236
[6] Olszewski P, Li J F, Liu D X and Walsh J L 2014 *J. Hazard. Mater.* **279** 60–6
[7] Mariotto D, Patel J, Svrcek V and Maguire P 2012 *Plasma Process. Polym.* **9** 1074–85
[8] Wu S, Wang Z, Huang Q, Lu X and Ostrikov K 2012 *Phys. Plasmas* **19** 103503
[9] Bruggeman P J *et al* 2016 *Plasma Sources Sci. Technol.* **25** 053002
[10] Jablonowski H and von Woedtke T 2015 *Clin. Plasma Med.* **3** 42–52
[11] Pekarek S 2012 *J. Phys. D: Appl. Phys.* **45** 075201
[12] Bruggeman P, Iza F, Lauwers D and Gonzalvo Y A 2010 *J. Phys. D: Appl. Phys.* **43** 012003
[13] Samukawa S *et al* 2012 *J. Phys. D: Appl. Phys.* **45** 253001

[14] Morfill G E, Shimizu T, Steffes B and Schmidt H-U 2009 *New J. Phys.* **11** 115019
[15] Shimizu T, Sakiyama Y, Graves D B, Zimmermann J L and Morfill G E 2012 *New J. Phys.* **14** 103028
[16] Shao T, Jiang H, Zhang C, Yan P, Lomaev M I and Tarasenko V F 2013 *Europhys. Lett.* **101** 45002
[17] Wang D, Zhao D, Feng K, Zhang X, Liu D and Yang S 2011 *Appl. Phys. Lett.* **98** 161501
[18] Nie Q Y, Cao Z, Ren C S, Wang D Z and Kong M G 2009 *New J. Phys.* **11** 115015
[19] Sun P P, Chen H L, Park S J, Eden J G, Liu D X and Kong M G 2015 *J. Phys. D: Appl. Phys.* **48** 425203
[20] Kong M G and Deng X T 2003 *IEEE Trans. Plasma Sci.* **31** 7
[21] Simor M, Rahel J, Vojtek P, Cemak M and Brablec A 2002 *Appl. Phys. Lett.* **81** 2716
[22] Williamson J M, Trump D D, Bletzinger P and Ganguly B N 2006 *J. Phys. D: Appl. Phys.* **39** 4400
[23] Liu Z C, Liu D X, Chen C, Li D, Yang A J, Rong M Z, Chen H L and Kong M G 2015 *J. Phys. D: Appl. Phys.* **48** 495201
[24] Cao Z, Nie Q, Bayliss D L, Walsh J L, Ren C S, Wang D Z and Kong M G 2010 *Plasma Sources Sci. Technol.* **19** 025003
[25] Cao Z, Walsh J L and Kong M G 2009 *Appl. Phys. Lett.* **94** 021501
[26] Tian W and Kushner M J 2014 *J. Phys. D: Appl. Phys.* **47** 165201
[27] Sakiyama Y, Graves D B, Chang H W, Shimizu T and Morfil G E 2012 *J. Phys. D: Appl. Phys.* **45** 425201
[28] Boxhammer V, Morfil G E, Jokipii J R, Shimizu T, Klämpfl T, Li Y F, Köritzer J, Schlegel J and Zimmermann J L 2012 *New J. Phys.* **14** 113042
[29] Wang B, Liu D, Zhang Z, Li Q, Wang X and Kong M G 2016 *IEEE Trans. Plasma Sci.* **44** 3295–301
[30] Tresp H, Hammer M U, Winter J, Weltmann K D and Reuter S 2013 *J. Phys. D: Appl. Phys.* **46** 435401
[31] De Geyter N, Morent R, Leys C, Gengembre L and Payen E 2007 *Surf. Coat. Technol.* **201** 7066–75
[32] Li D, Liu D X, Nie Q Y, Li H P, Chen H L and Kong N G 2014 *Appl. Phys. Lett.* **104** 204101
[33] Park J Y, Kostyuk P V, Han S B, Kim J S, Vu C N and Lee H W 2006 *J. Phys. D: Appl. Phys.* **39** 3805–13
[34] Machala Z, Janda M, Hensel K, Jedlovsky I, Lestinska L, Foltin V, Martisovits V and Morvova M 2007 *J. Mol. Spectrosc.* **243** 194–201
[35] van der Horst R M, Verreychen T, van Veldhuizen E M and Bruggeman P J 2012 *J. Phys. D: Appl. Phys.* **45** 345201
[36] Lu X, Jiang Z, Xiong Q, Tang Z and Pan Y 2008 *Appl. Phys. Lett.* **92** 151504
[37] Oehmigen K, Hahnel M, Brandenburg R, Wilke C, Weltmann K D and von Woedtke T 2010 *Plasma Process. Polym.* **7** 250–7
[38] Liu D X, Liu Z C, Chen C, Yang A J, Li D, Rong M Z, Chen H L and Kong M G 2016 *Sci. Rep.* **6** 23737
[39] Reuter S, Winter J, Schmidt-Bleker A and Tresp H 2012 *IEEE Trans. Plasma Sci.* **40** 2788–94
[40] Seinfeld J H 1986 *Atmospheric Chemistry and Physics of Air Pollution* (New York: Wiley)
[41] van Rens J F M, Schoof J T, Ummelen F C, van Vugt D C, Bruggeman P J and van Veldhuizen E M 2014 *IEEE Trans. Plasma Sci.* **42** 2622–3
[42] Lindsay A, Anderson C, Slikboer E, Shannon S and Graves D 2015 *J. Phys. D: Appl. Phys.* **48** 424007
[43] Williams M E and Darby J L 1992 *J. Environ. Eng.* **118** 988–93
[44] Winterbourn C C 1995 *Toxicol. Lett.* **82/83** 969–74
[45] Wu H, Sun P, Feng H, Zhou H, Wang R, Liang Y, Lu J, Zhu W, Zhang J and Fang J 2012 *Plasma Process. Polym.* **9** 417–24
[46] Yusupov M, Neyts E C, Simon P, Berdiyorov G, Snoeckx R, van Duin A C T and Bogaerts A 2014 *J. Phys. D: Appl. Phys.* **47** 025205
[47] Itikawa Y and Mason N 2005 *J. Phys. Chem. Ref. Data* **34** 1
[48] Pei X, Lu Y, Wu S, Xiong Q and Lu X 2013 *Plasma Sources Sci. Technol.* **22** 025023
[49] Jablonowski H, Bussiahn R, Hammer M U, Weltmann K-D, von Woedtke T and Reuter S 2015 *Phys. Plasmas* **22** 122008
[50] Gorbanev Y, O'Connell D and Chechik V 2016 *Chem. Eur. J.* **22** 3496–505
[51] Kurake N *et al* 2017 *J. Phys. D: Appl. Phys.* **50** 155202
[52] Darwent B D 1970 *NSRDS-NBS* **31** 48P